The 30 cm radio flux as a solar proxy for thermosphere density modelling

Thierry Dudok de Wit, Sean Bruinsma

J. Space Weather Space Clim., 7, A9 (2017)
DOI: 10.1051/swsc/2017008

SWSC

RESEARCH ARTICLE OPEN ACCESS

The 30 cm radio flux as a solar proxy for thermosphere density modelling

Thierry Dudok de Wit[1,*] and Sean Bruinsma[2]

[1] LPC2E, CNRS and University of Orléans, 3A avenue de la Recherche Scientifique, 45071 Orléans Cedex 2, France
[*]Corresponding author: ddwit@cnrs-orleans.fr
[2] CNES, Department of Terrestrial and Planetary Geodesy, 18 avenue E. Belin, 31401 Toulouse Cedex 4, France

Received 12 October 2016 / Accepted 15 February 2017

ABSTRACT

The 10.7 cm radio flux (F10.7) is widely used as a proxy for solar UV forcing of the upper atmosphere. However, radio emissions at other centimetric wavelengths have been routinely monitored since the 1950 s, thereby offering prospects for building proxies that may be better tailored to space weather needs. Here we advocate the 30 cm flux (F30) as a proxy that is more sensitive than F10.7 to longer wavelengths in the UV and show that it improves the response of the thermospheric density to solar forcing, as modelled with DTM (Drag Temperature Model). In particular, the model bias drops on average by 0–20% when replacing F10.7 by F30; it is also more stable (the standard deviation of the bias is 15–40% smaller) and the density variation at the the solar rotation period is reproduced with a 35–50% smaller error. We compare F30 to other solar proxies and discuss its assets and limitations.

Key words. Thermosphere density – Solar proxies – Solar radio emissions

1. Introduction

The solar radio flux at 10.7 cm (F10.7) is a widely, if not the most widely used index of solar activity: this quantity describes solar UV forcing of the upper atmosphere and is measured daily since 1947 (Floyd et al. 2005; Tapping 2013). Many operational space weather models and also climate models use the F10.7 index as their prime solar input. The widespread use of F10.7 can be partly ascribed to its high radiometric accuracy and stability, which are essential for assessing variations on time scales of days to decades. In addition, F10.7 is measured from the ground. Direct (space-borne) UV observations in comparison cannot meet such accuracy and stability requirements (BenMoussa et al. 2013); their limitations have spurred a long quest for proxies that mimic the variability in specific spectral bands of the UV and therefore may describe more properly the solar energy absorbed in the upper atmosphere (e.g. Tobiska et al. 2008). For operational applications in space weather, these requirements become even more stringent because near real-time and continuous access to the data are needed (Lilensten et al. 2008). In this context, radio fluxes are and remain prime candidates for studies that require solar UV inputs. Particular attention will be given here to satellite drag modelling for satellite operators. Satellite drag is proportional to the thermospheric neutral density, whose variations are mainly driven by the solar UV flux and by geomagnetic activity (Emmert 2015b). Although F10.7 is the most commonly used indicator of thermospheric density variations on time scales of several months and beyond, the reasons leading to the better efficacy of F10.7 have remained elusive.

Surprisingly, little is known about the relevance of radio fluxes at wavelengths other than 10.7 cm. Emissions occurring at centimetric wavelengths are highly correlated on monthly and yearly time scales because they are all eventually driven by the solar magnetic cycle. On daily to weekly time scales, however, they start exhibiting subtle differences (Schmahl & Kundu 1998). At even shorter time scales, corresponding to transients such as solar flares, the differences become much more pronounced (Pick & Vilmer 2008).

Several observatories have been routinely monitoring the Sun at various wavelengths. The USAF Radio Solar Telescope Network, for example, is widely used to monitor flares (Gary & Keller 2004). The Toyokawa and Nobeyama observatories (Tanaka, 1967) stand out by continuously providing daily averages at several wavelengths since 1951 with high radiometric accuracy. In a previous study (Dudok de Wit et al. 2014) we already described these data and showed how the radio flux at 30 cm (henceforth called F30) provides a valuable complement to F10.7. By replacing F10.7 with F30 in the construction of the thermosphere model DTM2013 (Drag Temperature Model; Bruinsma 2015) the errors were reduced significantly.

The objective of this paper is to advocate the F30 index as a new solar proxy for solar UV emissions, with special relevance to thermosphere density modelling. This index thereby complements other proxies such as F10.7 and the MgII core-to-wing index (Viereck et al. 2001), which describe other aspects of the UV variability. We concentrate on time scales of days to decades; short transients such as flares and bursts require a different approach and are beyond the scope of our study.

Following this introduction, we first provide a physical motivation for using the 30 cm radio flux (Sect. 2) and then describe the data and their preprocessing (Sect. 3). We then compare F30 to other UV proxies (Sect. 4) and to the globally-averaged thermospheric density (Sect. 5). Finally we evaluate its performance by comparing two test versions of the DTM, one constructed with F10.7 and the other with F30 (Sect. 6), and conclude in Section 7.

2. What distinguishes F30 from F10.7?

Solar microwave emissions comprise contributions from various physical processes. If we exclude transients such as flares, which are dominated by non-thermal emissions, then the main contributions are incoherent thermal free-free and gyroresonance emissions (Kundu 1965; White & Kundu 1997). The former prevail in cool dense plasmas, including the quiet Sun, but are also emitted by coronal loops, faculae, etc. Gyroemissions dominate above sunspots with intensive magnetic fields. Propagation effects blur this simple picture; gyroemissions, for example, involve many resonances whose contribution is conditioned by the optically thick overlying free-free emission.

These two contributions have different spectra. For free-free emissions, the spectrum decreases monotonically as the wavelength squared and thus is more intense at 10.7 than at 30 cm. Gyroresonant processes lead to a more complex spectrum, which on average peaks around 10 cm (Tapping & Detracey 1990). These processes have their counterpart in the UV part of the spectrum (White et al. 2011). As a first approximation, variations in gyroresonance emissions are more closely connected to those observed in the Extreme-UV (EUV, 1–120 nm) band of the solar spectrum because both are associated with sunspots. Conversely, free-free emissions are more strongly correlated with Far-UV (FUV, 120–200 nm) and Middle-UV (MUV, 200–300 nm) emissions.

These different emissions and their connection to the UV spectra justify the large interest in multi-wavelength radio observations for a better understanding of the underlying physics (Schmahl & Kundu 1998) and for designing proxies that may reproduce solar UV forcing more accurately. In (Dudok de Wit et al. 2014) we investigated that idea and showed that the variability in the radio flux, as observed at five wavelengths (3.2, 8.0, 10.7, 15.0 and 30.0 cm), can be statistically decomposed into three independent contributions, two of which closely match the expected physical emission mechanisms. The third and weakest contribution describes non-thermal emissions associated with major active regions. That analysis showed that wavelengths longward of 10.7 cm receive a larger contribution from solar features other than active regions, which turn out to be better correlated with less energetic bands of the UV, namely FUV and MUV.

Why consider F30 specifically as a new index? There are two alternatives: first we could consider multi-wavelength radio observations and by physical or empirical modelling combine these into a new proxy. This approach is physically more appealing, but requires multiple observations, which presently come from different instruments, thus multiplying the risk of having calibration issues, outages and outliers. A second, simpler and more robust strategy consists in selecting the accurately calibrated radio flux at one particular wavelength, exactly in the way F10.7 is used, under the condition that it provides a more pertinent blend of contributions. With space weather applications in mind, we favour here the second approach, while being aware that it is suboptimal and that synoptic radio monitoring with one single instrument (e.g. Tapping & Morton 2013) is the way forward.

Several limitations constrain the range of centimetric wavelengths that can be meaningfully considered for making UV proxies. Emissions below 3 cm are increasingly absorbed by the Earth's atmosphere and therefore are not suitable for long-term monitoring. Emissions above 50 cm receive a growing contribution from coherent plasma emissions, which do not have a direct UV counterpart. The spectral band of interest thus ranges approximately from 3 to 50 cm, in which we found the flux at 30 cm to offer a good compromise for describing solar forcing of the upper atmosphere (Dudok de Wit et al. 2014).

3. The radio data

Among the observatories that monitor the Sun in centimetric wavelengths, the Ottawa/Penticton (Tapping 2013) and Toyokawa/Nobeyama (Tanaka 1967) observatories stand out by providing long and continuous records of daily averages with excellent radiometric quality. The former[1] started monitoring the 10.7 cm flux on 14 February 1947. The latter[2] provides several wavelengths, including 30 cm, since 1 March 1957. Both instruments are calibrated at least once per day, always using the same protocol since measurements started. The Ottawa facility was relocated to Penticton in May 1991 and the Toyokawa facility was relocated to Nobeyama in May 1994. Thanks to a temporary overlap, this has not significantly affected the observations. More details regarding these data sets are given by Dudok de Wit et al. (2014).

Both the F10.7 and F30 indices are in principle devoid of flares, although they are processed in different ways. For F10.7, the flare-less component is estimated from three daily observations, whereas for F30, the flux is continuously monitored from sunrise till sunset. For Ottawa/Penticton, the time stamp is typically 20:00 UT and the data become accessible before 24:00 UT. For Toyokawa/Nobeyama, the time stamp is typically 3:00 UT and the provisional value comes out around 12:00 UT. Their definite values are delivered once per month, with a latency of 15–40 days. Both indices are thus available in a timely manner for operational use. However, resampling in time may be necessary for performing detailed comparisons.

Fortunately, missing values or outliers are very rare. Since January 2000, six missing values have been reported in F10.7 and 21 in F30. To ease the access to multi-wavelength data from Toyokawa/Nobeyama, we provide a consolidated dataset with all wavelengths, interpolated data gaps and also a 30-day forecast at http://spaceweather.cls.fr.

Figure 1 displays the two indices, showing their high correlation. The excerpt reveals subtle differences between the two, which are most evident during the Halloween event of October 2003. The emergence of a major sunspot group near October 30 causes both fluxes to increase sharply. However, the increase is more noticeable in F10.7 because it receives a larger contribution from gyroresonance emissions. Conversely, one and two solar rotations later, when the sunspot group has become less active and F10.7 has dropped, F30 continues to stay at a relatively high level because of the presence of bright faculae and coronal loops.

An important issue is the precision and stability of these records, for which detailed numbers are lacking. Precision refers here to random errors that would affect the radio flux if the Sun were perfectly stable. We estimate it by using an autoregressive model approach similar to that described by Dudok de Wit et al. (2016). The precision increases with the

[1] Data are available at ftp://ftp.ngdc.noaa.gov/STP/space-weather in the directory /solar-data/solar-features/solar-radio/noontime-flux/penticton/.

[2] Data are available at http://solar.nro.nao.ac.jp/norp/html/daily_flux.html.

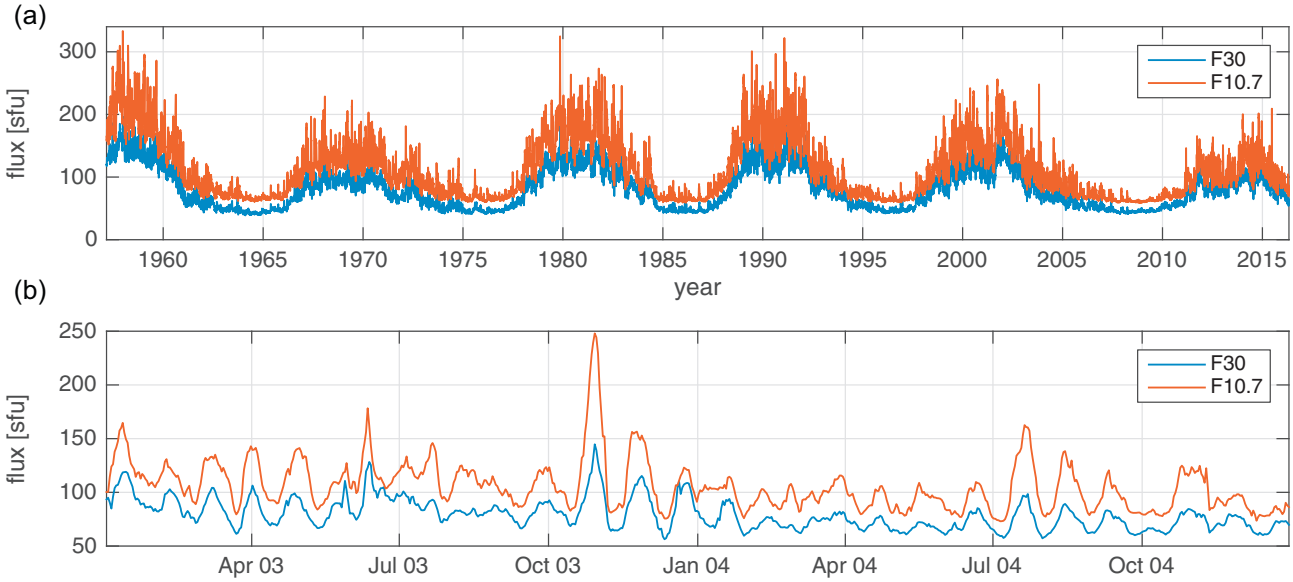

Fig. 1. Original values of F30 and F10.7 since 1 March 1957, when the F30 series starts. (a) Full record, and (b) a two-year excerpt with the Halloween event of October 2003.

Table 1. Precision of the radio indices. Values are expressed in solar flux units [sfu].

Index	$1-\sigma$ precision [sfu]
F30	$\sigma = 0.034 \times \mathrm{F30} - 0.71$
F10.7	$\sigma = 0.053 \times \mathrm{F10.7} - 2.35$

level of activity, similarly to what is observed with most solar proxies, such as the sunspot number. These values are listed in Table 1. The important result here is the relatively modest value of the precision, which is of the order of 3–4% for both indices.

Estimating the stability is much more challenging and formally requires an external reference. However, since the F10.7 and F30 indices are measured totally independently, some information may be gleaned from their difference. In Figure 2 we rescale F30 to F10.7 by using a quadractically nonlinear transform and then display their difference. Interestingly, this difference mostly consists of short-term fluctuations, with a weak but significant linear trend. The former can be ascribed to differences in the physical emission processes, while the linear trend is most likely instrumental. Similar linear trends, all having the same sign, are observed between F10.7 and fluxes at other wavelengths from Toyokawa/Nobeyama whereas none can be detected between different wavelengths from the same Toyokawa/Nobeyama observatory. The trend between F10.7 and F30 equals −0.21 [sfu/year], which gives us an indication of the stability. Such a small value is negligible for most space weather applications, but does matter for space climate studies.

4. Comparison with solar proxies

We now compare F30 with a set of solar UV proxies to improve our understanding. In the next section we shall compare it directly to thermospheric density observations. There exist many UV proxies (Ermolli et al. 2014), each of which preferentially describes a spectral band or a class of solar features. Those proxies which have been specifically recommended for drag modelling (e.g. Bowman et al. 2006) are:

- F10.7, which is used in all thermosphere models;
- the MgII core-to-wing index, which is used in many studies for the forcing of the upper atmosphere (Lean et al. 2006) and also in the DTM2000 thermosphere model (Bruinsma et al. 2003). We use the Bremen composite[3], whose record starts on 7 November 1978.
- the EUV flux, integrated from 26 to 34 nm, by the Solar EUV Monitor (SEM) radiometer[4] on board SOHO (Hovestadt et al. 1995). These data represent the first long-term measurements of EUV irradiance; they are available since 1 January 1996 and are used in the JB2008 drag model (Bowman et al. 2008).

Many authors have evaluated the efficacy of these proxies for thermospheric modelling, see the review by Emmert (2015b). While the EUV flux from SEM and the MgII index perform slightly better at time scales of a few months and below, F10.7 is still preferred by most for its good overall results and for its long-term stability. Incorporating several proxies improves model results, but the statistical significance of adding more solar inputs is limited (Dudok de Wit & Bruinsma 2011).

All these proxies are highly correlated on the long term because they are driven by solar magnetism. Figure 3 illustrates this for a two-year interval. Their strong similarity is usually quantified by means of Pearson's correlation coefficient. This quantity, however, is of little benefit because its large value is highly dominated by the coherent solar cycle modulation. More pronounced differences arise on shorter time

[3] Available at http://www.iup.uni-bremen.de/gome/solar/MgII_composite.dat.
[4] Available at http://www.usc.edu/dept/space_science/sem_data/sem_data.html.

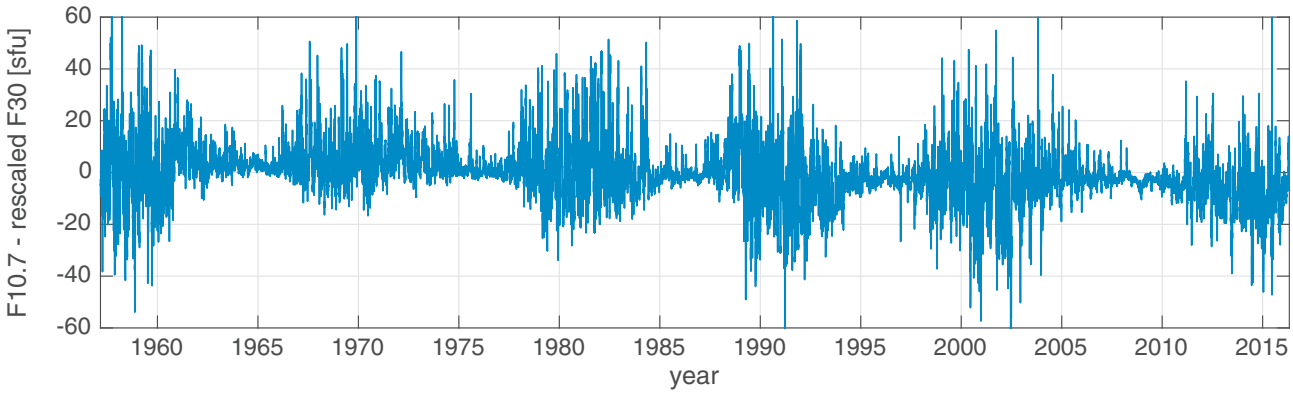

Fig. 2. Difference between F10.7 and F30 after rescaling the latter to F10.7 by using a quadratically nonlinear model. A weak but significant downward trend is apparent, with an average slope of -0.21 [sfu/year].

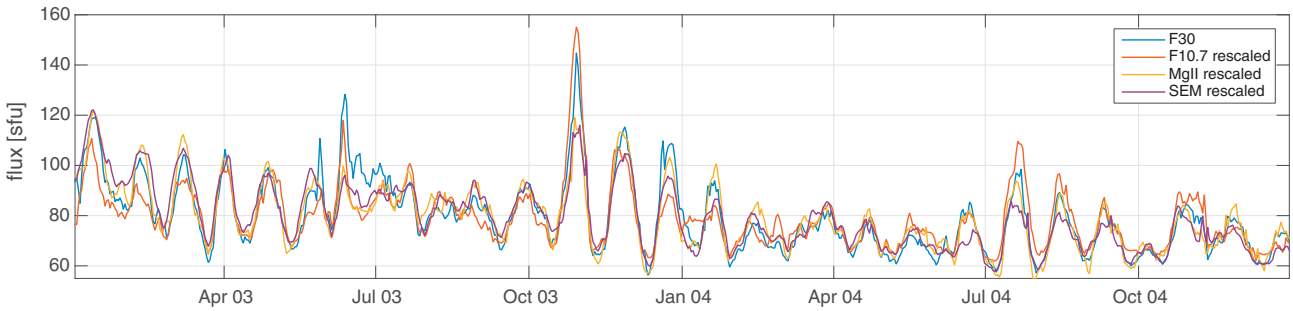

Fig. 3. Excerpt showing F30, F10.7, MgII and SEM. The latter three are rescaled to F30 by using a quadratically nonlinear model in order to reveal their similarities.

scales, typically at those that correspond to the lifetime of active regions (weeks to months). Before we address these, however, let us first consider the longest time scales because they are important for assessing long-term stability.

To investigate possible drifts in the observations, we apply a procedure that is routinely used in solar radiophysics and remove the signature of solar rotational modulation (Kundu 1965; Schmahl & Kundu 1998). We keep the lower envelope only (called B component in that context) by applying a filter that keeps the minimum in a 27-day moving window. In Figure 4 we use a scatter plot to compare the lower envelope of F30 with that of the other proxies. A first conspicuous result is the close-to-linear relationship between these different quantities, which suggests that the solar cycle has the same imprint on all. A second result is the highly time-invariant relationship between F30 and F10.7, and between F30 and MgII. There is no indication for a drift either, except for the weak aforementioned linear trend detected between F30 and F10.7. The situation is quite different with SEM, whose larger scatter is the consequence of a downward trend that started during solar cycle 23. Whether this trend is instrumental or not is an open question; meanwhile, SEM cannot be rescaled to F30 with a time-invariant function.

Dudok de Wit et al. (2009) and Dudok de Wit & Bruinsma (2011) have shown that no single proxy can properly reproduce the UV variability at all time scales. Let us therefore build a more global picture and compare our different quantities scale-wise. The proper quantity for doing this is the cross-coherence function (Bendat & Piersol 2000). Let $y_i(t)$ be a proxy record and $y_i(\omega)$ its Fourier transform. The cross-coherence is then defined as

$$C_{ij}(\omega) = \frac{\langle y_i(\omega) y_j^*(\omega)\rangle}{\sqrt{\langle |y_i(\omega)|^2\rangle}\sqrt{\langle |y_j(\omega)|^2\rangle}}, \quad (1)$$

where $\langle \ldots \rangle$ denotes ensemble-averaging. In the following we estimate the Fourier transform by continuous wavelet transform, using Morlet wavelets, and replace ensemble-averaging by an average over time.

The main quantity of interest is the modulus $|C_{ij}|$ of the cross-coherence, which varies from 0 (no correlation at that particular frequency) to 1 (total correlation). Figure 5a shows the cross-coherence between F30 and the other proxies, and the lower one between F10.7 and the other proxies. All values drop to 0 at high frequency because small-scale variations, whether solar or instrumental, are mostly uncorrelated. The cross-coherence then peaks at the solar rotational period of 27 days. This was to be expected because solar rotation coherently modulates all quantities. Interestingly, at that period, F30 is better correlated with other proxies than F10.7 is. In particular, F30 and MgII are highly correlated. This similarity also applies to the first harmonic of this 27-day solar rotational period, which is partly related to projection effects. For time scales in excess of one month, the cross-coherence gradually reaches 1, with no significantly different performance.

We could equally well consider the cross-phase (the argument of the cross-coherence), which describes the phase lag between the proxies. We skip it here because it is not significantly different from 0 and hence all quantities vary in phase.

To summarise, the largest values of the cross-coherence are obtained for the F30-MgII pair, especially at solar rotational

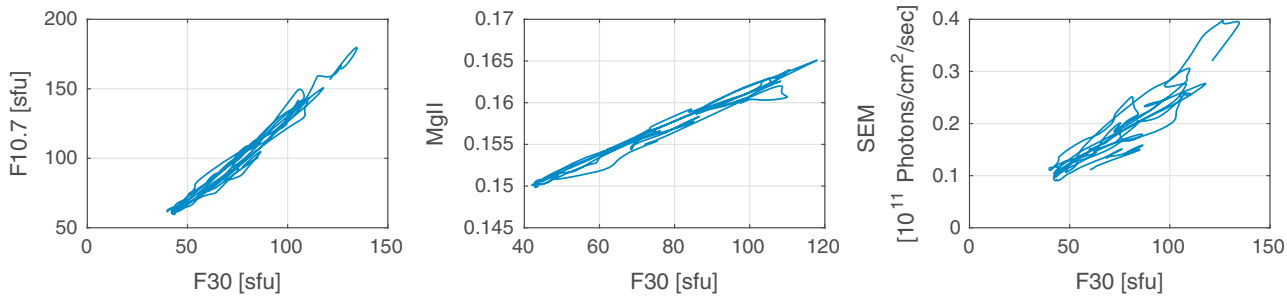

Fig. 4. Scatter plot between the lower envelope of F30 and that of the other proxies. The lower envelope has been averaged over 180 days to ease visualisation.

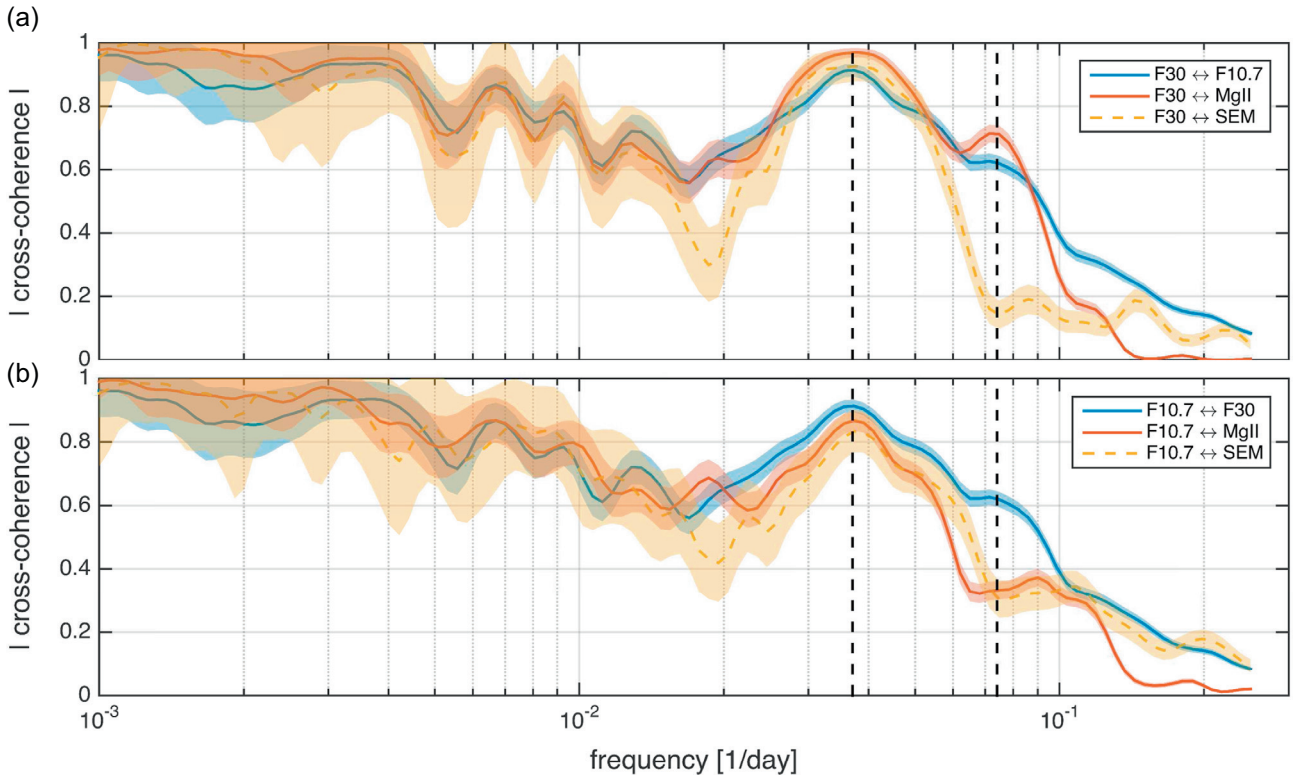

Fig. 5. Modulus of the cross-coherence between three proxies (F10.7, MgII and SEM) and F30 (a), and F10.7 (b). Coloured bands correspond to a $\pm\sigma$ confidence interval. The 27-day and 13.5-day periods are indicated by dashed lines. The time intervals used for estimating the cross-coherence are proxy-dependent: solar cycles 20–24 for radio proxies, cycles 21–24 for the MgII index, and cycles 23 and 24 only for SEM. For that reason, the different cross-coherences are not strictly comparable.

time scales, thus confirming that F30 receives a larger contribution than F10.7 from solar features other than sunspots. This result is important for satellite drag applications because of the high variability of the thermospheric density at those time scales. In addition, the MgII index has been found to be a better proxy for the 27-day density response than F10.7 (Lean et al. 2006) and so we may expect F30 to be relevant as well for the density. This will be investigated in the next section.

5. Comparison with the thermospheric density

Let us now compare the solar UV proxies with the thermospheric density and do so again on a scale-by-scale basis. The relationship between average solar forcing and average density is nonlinear but monotonic (Emmert 2015b), which allows us again to rely on the convenient framework of the cross-coherence. The true picture, however, is blurred by the contribution of geomagnetic activity, which also strongly affects the density, but does so more intermittently and mostly independently of the UV flux. For these reasons, the impact of geomagnetic activity can be approximated as a random driver that mostly affects short time scales of approximately ten days and below.

While a lowpass filter is able to remove most of the geomagnetic activity, it cannot fully eliminate the impact of recurrent storms. We tried to further remove the latter by using an empirical transfer function model (Dudok de Wit & Bruinsma 2011) to describe the solar radiative and the geomagnetic forcings. By then running the same model with geomagnetic forcing set to zero, one can estimate by how much geomagnetic activity contributes to the observed density variations. The differences we observed in the cross-coherence

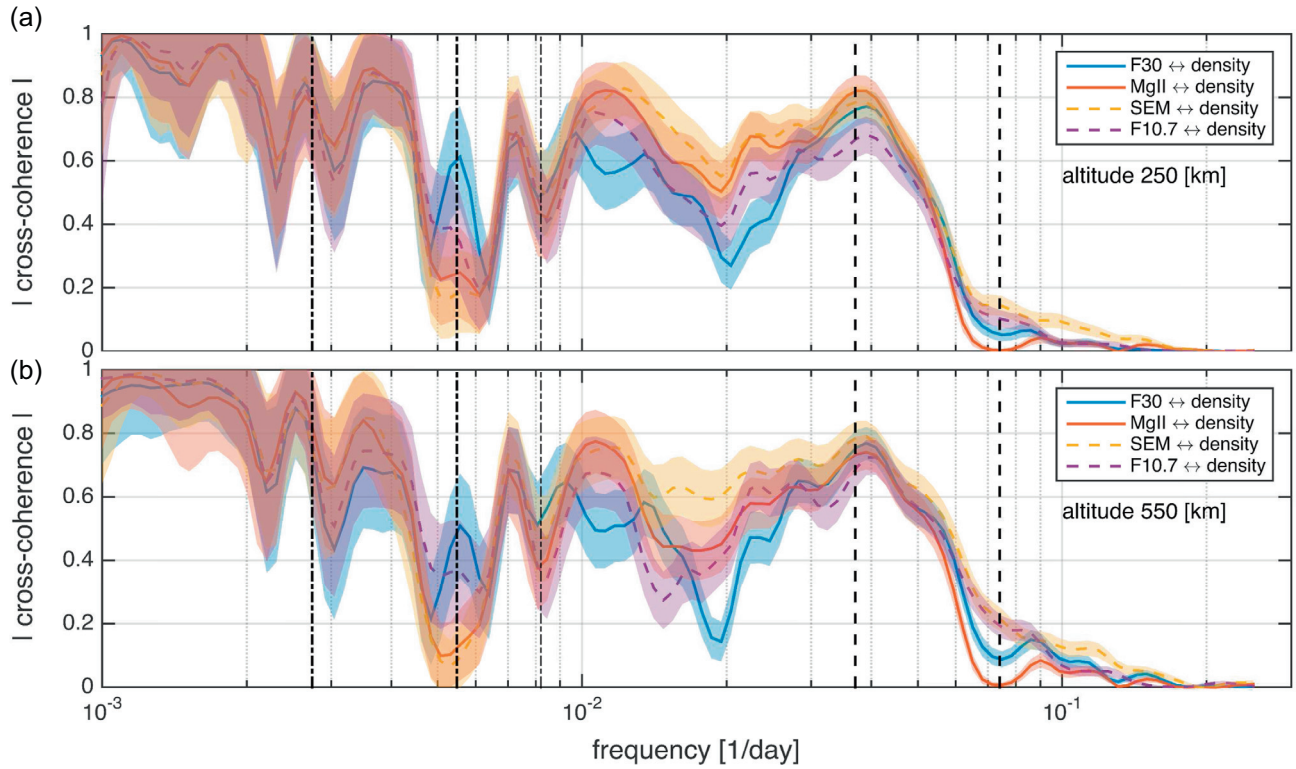

Fig. 6. Modulus of the cross-coherence between three proxies (F30, MgII, SEM and F10.7) and the thermospheric density at 250 km altitude (a), 550 km altitude (b), from 1996 to 2011. Coloured bands correspond to a ± σ confidence interval. The 27-day and 13.5-day periods, and periods associated with seasonal variations are indicated by dashed lines.

were small as compared to the assumptions that had to go into this additional layer of modelling. For that reason, we prefer here to rely on a simple lowpass filter while being aware that it is open to improvement.

We use a dataset of globally-averaged densities computed by Emmert (2009, 2015a). The data cover the period from 1967 to 2011 at heights from 200 to 600 km. The thermospheric density exhibits various seasonal oscillations of one year and its harmonics, which are not present in solar proxies. These periodicities require a climate model in order to be properly described and corrected for in the cross-coherence. For that reason, in the results that follow, we systematically ignore seasonal variations and concentrate on the remaining time scales. Likewise, we also ignore the shortest time scales, which are predominantly affected by geomagnetic activity. Note that because of these effects, the values of the cross-coherence are likely to be underestimated.

Figure 6 compares the cross-coherence between our three proxies (and F30) and the density respectively at 250 km and at 550 km. To facilitate their direct comparison, we restrict the time interval to 1996–2011, when all the proxies and the density are available simultaneously. The relative amplitude of solar-driven density variations increases with altitude and so should the signal-to-noise ratio of the cross-coherence. As expected, the cross-coherence rapidly drops to zero for time scales below approximately ten days because of geomagnetic activity. Likewise, pronounced dips occur at periods of one year and its harmonics.

Figure 6 shows that the proxies offer comparable performance, given the uncertainties in the cross-coherence. However, SEM slightly outperforms the others between time scales from one to several solar rotations. For the 27-day variation, which is of particular interest because of its high cross-coherence, F30 is preferable to F10.7.

The picture that emerges here is again a small but significant advantage of F30 over F10.7. The good performance of SEM suggests again that direct UV measurements ultimately are the best solution for describing solar forcing of the upper atmosphere. However, since such direct observations are not yet reliable enough and since SEM suffers from a drift that is not observed in the thermospheric density, proxies are still the preferred option for space weather applications.

6. Model performance with F30 and F10.7

To further test the F30 index, we now compare a thermosphere model constructed with the 30 cm flux with one constructed with the 10.7 cm flux, similarly to what we did in (Dudok de Wit et al. 2014). Both models are based on the exact same density data, which is the DTM2013 database without the high-resolution, high-accuracy density data in the low-altitude range of 230–270 km of the Gravity field and steady-state Ocean Circulation Explorer (GOCE; Bruinsma et al. 2014). The database does notably contain total neutral densities inferred from high-resolution, high-accuracy accelerometer measurements on the Gravity Recovery and Climate Experiment (GRACE) in the 450–500 km altitude range from April 2003 to December 2010, and Stella daily mean densities at about 800 km altitude from 1993 to December 2010. The complete GOCE (November 2009–October 2013), GRACE (April 2003–December 2015) and Stella (January 2000–April 2013) datasets are used to evaluate model performance because of their complementary altitude coverage. This kind of comparative test allows quantifying the improvement due to F30 after a

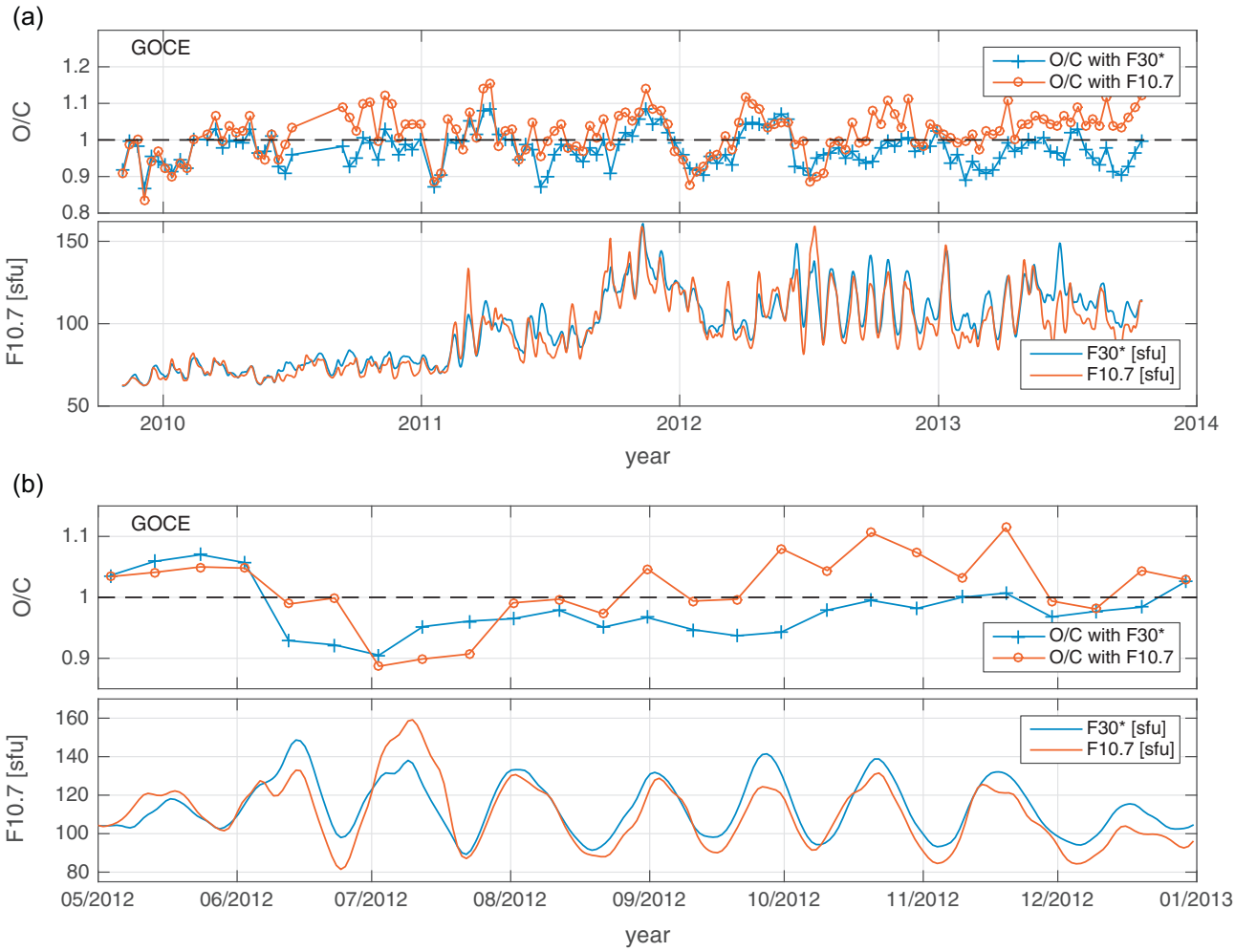

Fig. 7. 10-day averaged GOCE density ratios (O/C) obtained with the F10.7 and F30* thermosphere models and the daily F10.7 and F30* proxies. (a) Full record and (b) zoom on the period May–December 2012.

full modelling effort, which is more pertinent (and generally more conservative) than what can be obtained by simply correlating or modelling the time series of a single density dataset with a solar proxy, as done in Section 5. Such a test is more pertinent than a correlation analysis because of:

- inconsistencies between density datasets due to scale errors, which modellers correct for as well as possible by means of data preprocessing or estimation of scale factors;
- the more complex way to reproduce total density by summing the contributions of the main constituents (N_2, O_2, O, He, H), which propagates scale errors in density to all altitudes.

We evaluate the solar proxies for use in thermosphere models and as such this test does provide realistic numbers of improvement that can be achieved; the comparison with the density time series at a constant altitude performed in Section 5 should be considered as an ideal case when all datasets are consistent.

Fast variations of the solar flux (on time scales of typically one solar rotation and below) do not impact the thermosphere in the same way as slower variations. To account for this effect, it is customary for models to use two solar inputs (Hedin et al. 1977): slow variations are represented by a trend, defined as the running mean of the flux over the last 81 days, while fast variations are described by the detrended flux, i.e. the difference between daily values and trend.

In the following, we run the two dedicated F10.7 and F30 test models respectively with the F10.7 index and with the F30 index, after linearly rescaling the latter to F10.7. We obtain the rescaled F30, hereafter denoted F30*, by total least squares fitting, which gives $F30^* = 1.554 \times F30 - 1.6$.

The quantity we use for model evaluation is the observed-to-model density ratio (O/C), called density ratio in the following, because it allows comparison of relative model precision independent of (orders of magnitude) altitude variations. The density ratios are then averaged every 10 days, which attenuates variations due to geomagnetic activity and density variations on time scales of a solar rotation and longer can be analysed. This is a pertinent choice, because solar cycle variations, followed by solar rotation variations in EUV emissions, have the largest modulating effect on density due to solar irradiance.

Figure 7a presents the 10-day averaged GOCE density ratios obtained with the F10.7 and F30* thermosphere models, as well as the daily F10.7 and the F30* proxies. The mean of the O/C density ratios using all data is very good for both models: we find 1.019 and 0.974 with F10.7 and

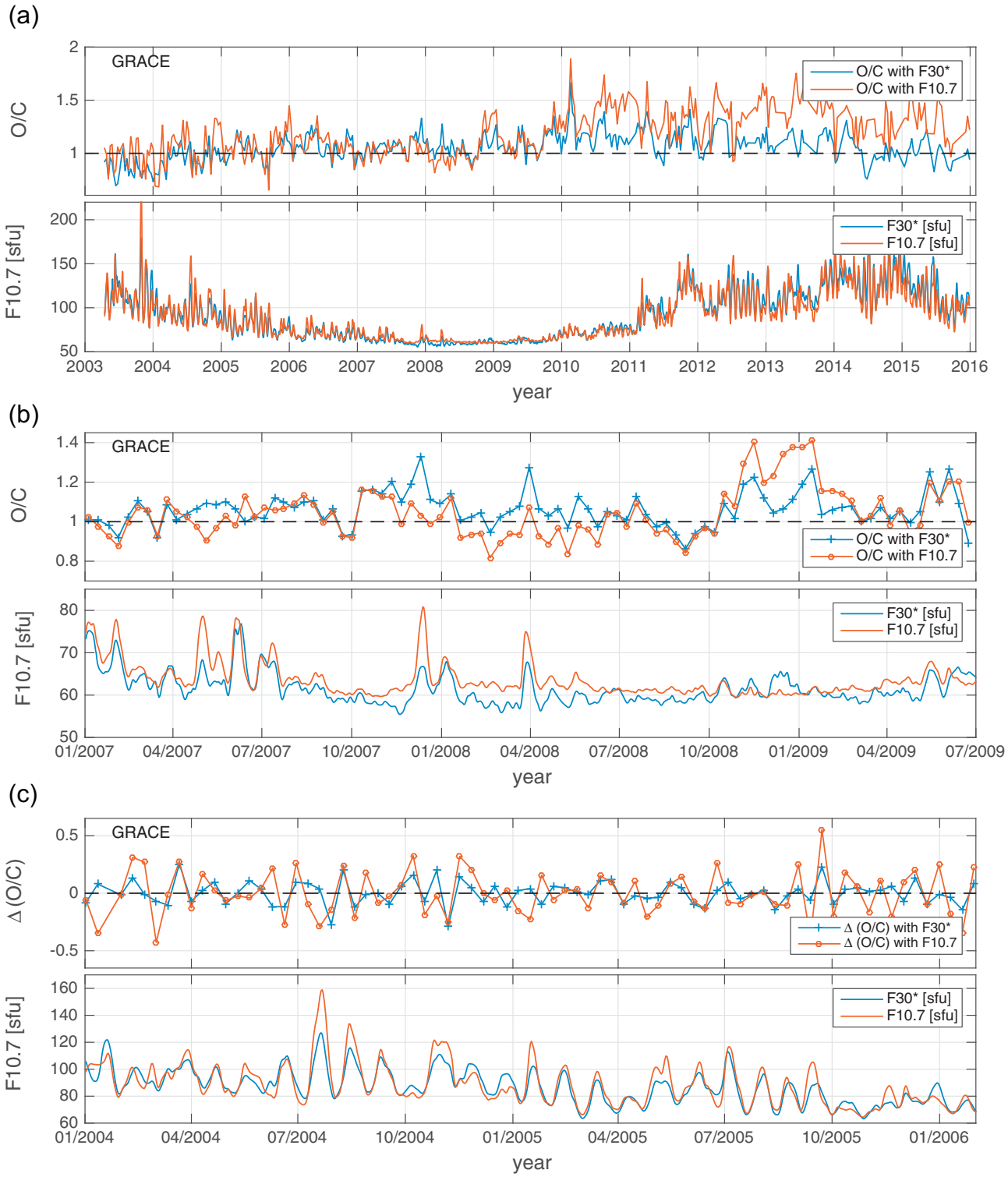

Fig. 8. 10-day averaged GRACE density ratios (O/C) obtained with the F10.7 and F30* thermosphere models and 81-day mean F10.7 and F30* proxies. (a) Full record, (b) zoom on the period January 2007–June 2009 and (c) the differenced density ratio Δ(O/C) (see Eq. 2) for the period January 2004–December 2005.

F30*, respectively. However, the standard deviation of the density ratio is clearly in favour of the latter, with 0.061 compared to 0.046. That is, both proxies give negligible bias, whereas the density ratios with F30* vary less around the mean because the densities are better reproduced than with F10.7.

The root mean square (RMS) of the density ratio minus one $\sqrt{\langle((\mathrm{O/C})(t)-1)^2\rangle}$ is a global measure of model performance, and geophysical and instrumental noise in the observations. We find 0.123 and 0.113 with F10.7 and F30*, respectively. These statistics demonstrate better performance with F30*. However, comparing over shorter periods with clear

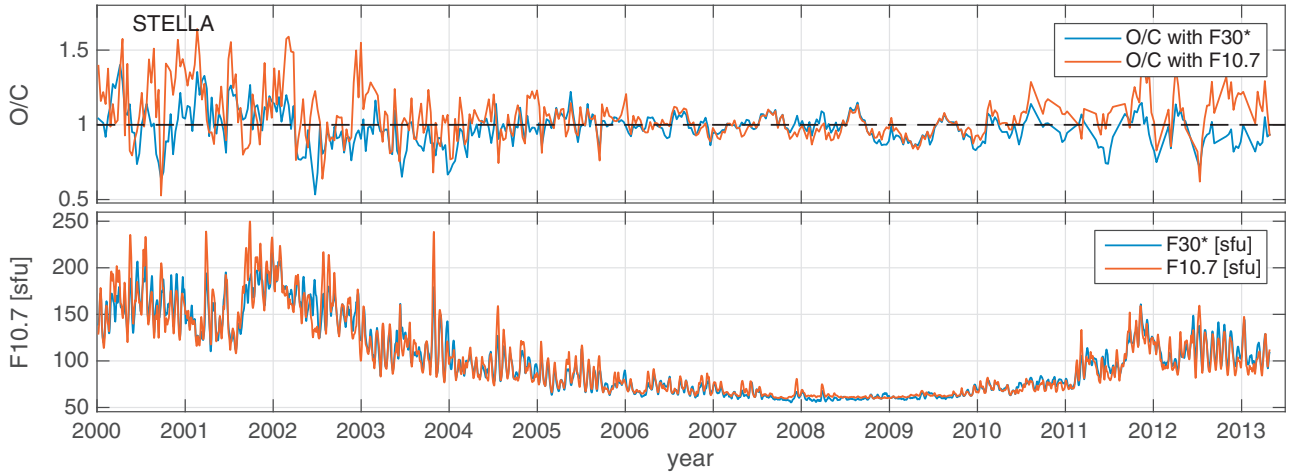

Fig. 9. 10-day averaged Stella density ratios (O/C) obtained with the F10.7 and F30* thermosphere models and 81-day mean F10.7 and F30* proxies.

solar rotation variations makes a more compelling case. This is evident from Figure 7b, which shows an excerpt of period May–December 2012 with seven high amplitude solar rotation variations. The figure also shows that F30* is not always the better proxy: the first high solar rotation peak (after June 2012) in F30* is about 15 sfu higher than the corresponding peak in F10.7, which leads to a large drop of about 0.10 (from 1.05 to 0.93) in the F30* model density ratio and about half that for the F10.7 model.

From August to December 2012 the F30* model reproduces density more accurately: the mean density ratio is slightly less than one with small standard deviation, and the solar rotation period is hardly present. The density ratios of the F10.7 model on the other hand are clearly tracking the solar rotation modulation in the F10.7 flux. Here, the amplitude of F10.7 is too small, which leads to the F10.7 model to predict a too low density by about 5–8%.

Figure 8a presents the 10-day averaged GRACE density ratios computed with the F10.7 and F30* thermosphere models, and the 81-day mean of the F10.7 and the F30* radio fluxes. The mean of the density ratios using all data is good for the F30* model, even if there are some offsets visible, in particular in 2003. The F10.7 model cannot reproduce the densities without significant bias after 2010, reaching 50–60% for periods that F10.7 is 10–20 sfu lower than F30*. The mean (RMS) of the density ratios using all data is 1.172 (0.321) and 1.061 (0.233) with F10.7 and F30*, respectively; for the period April 2003–December 2009 (2010–2015) the mean and standard deviation of the density ratios is 1.056 and 0.143 (1.352 and 0.172) and 1.022 and 0.119 (1.105 and 0.132), respectively. So it appears that we have two distinct periods: for the first period, both models predict density with rather small biases on average, but from about 2010 onwards both models are underestimating density systematically. However, with F30* the underestimation is limited to 11% on average, whereas with F10.7 it is three times larger, namely 35%.

Differences in the radio flux are rather small during the solar minimum spanning from late 2007 to 2009, except for two rotations. However, the effect on density is clearly visible in Figure 8b. Fluxes and density ratios are quite similar the first few months, before October 2007. The two peaks just before 2008 and around April 2008 are high for both proxies, but 10–15 sfu higher in F10.7. For both peaks, the density ratios of the F10.7 model change less from one point to the next than for the F30* model. For this, we define the differenced density ratio

$$\Delta(\mathrm{O/C})(t) = \mathrm{O/C}(t) - \mathrm{O/C}(t + 10\,\mathrm{days}) \qquad (2)$$

Using this quantity we find that the F10.7 model reproduces the densities for this short period with higher fidelity, i.e. higher F10.7 amplitudes are more representative of upper atmosphere heating. Over the longer period of 6 months from January 2008 to June 2008 however, the F10.7 flux is somewhat higher than F30*, which results in overestimating densities.

A period of significantly higher F30* is visible from November 2008 to January 2009, but the F30* model density ratios still increase (underestimation) by some 20% to 1.2–1.25. Over the same period, the F10.7 density ratios increase twice that number to about 1.40. Both proxies seem to be too weak for that period, but F30* is performing convincingly better. For these years, F30* and F10.7 have alternating performance: the average and standard deviation of the density ratios with F30* (F10.7) is 1.068/0.089 (1.051/0.139). Another way to express the model quality is by accumulating the absolute values of Δ(O/C): 4.67 with F30* and 4.80 with the F10.7 model.

Figure 8c displays the Δ(O/C) from 2004 to 2006. These are years during which the solar rotation modulation of the flux was considerable. Visual inspection reveals that both models have remaining errors at the solar rotation period, but that the effect is much smaller with the F30* model: the accumulated absolute values of Δ(O/C) (respectively, mean and standard deviation of the density ratios) are 5.9 (0.989/0.107) with F30* and 10.8 (1.050/0.160) with the F10.7 model.

The Stella data is at the highest altitude of the three datasets used here. We have used data over the duration of an entire solar cycle, overlapping GOCE and GRACE, and in addition the maximum years of cycle 23, which is much stronger than the current cycle 24. Figure 9 presents the 10-day averaged Stella density ratios computed with the F10.7 and F30* thermosphere models, and the 81-day mean of the F10.7 and the F30* radio fluxes. The Stella and GRACE density ratios are rather comparable, especially after 2010, but they are smaller with Stella because they are lowpass filtered in the density

Table 2. Model comparisons to GOCE, GRACE and Stella density data, and solar activity as represented by the F10.7 and F30* radio fluxes; F stands for either F10.7 or F30*. The columns respectively describe: the dataset, the time average ($\langle O/C \rangle$) and the standard deviation ($\sigma_{(O/C)}$) of the density ratio, the sum of the unsigned differenced density ratio for the given time interval ($\sum|\Delta(O/C)|$), the mean radio flux ($\langle F \rangle$), its standard deviation (σ_F) and the standard deviation of the detrended flux ($\sigma_{F-\bar{F}}$), obtained by subtracting a 81-day mean.

Dataset	$\langle O/C \rangle$	$\sigma_{(O/C)}$	$\sum\|\Delta(O/C)\|$	$\langle F \rangle$ [sfu]	σ_F [sfu]	$\sigma_{F-\bar{F}}$[sfu]
GOCE F10	1.019	0.061	6.2	105.6	24.3	15.3
GOCE F30*	0.975	0.046	4.5	113.3	25.6	14.1
GRACE F10 (all)	1.180	0.213	51.3	100.9	29.9	16.6
2003–2009	1.056	0.143	27.0	86.9	23.9	14.6
2010–2015	1.352	0.172	24.3	116.6	28.2	18.6
GRACE F30* (all)	1.057	0.132	34.3	105.9	32.6	14.3
2003–2009	1.022	0.119	19.4	87.9	23.5	11.4
2010–2015	1.105	0.132	15.0	126.2	29.3	16.9
Stella F10 (all)	1.055	0.162	48.4	113.4	45.6	19.7
2000–2002	1.143	0.236	20.5	180.1	33.5	30.2
2010–2013	1.091	0.137	8.7	105.8	24.8	15.9
Stella F30* (all)	0.977	0.117	31.0	117.0	46.1	16.1
2000–2002	1.013	0.172	11.5	185.5	28.0	23.6
2010–2013	0.950	0.100	5.6	112.4	25.5	14.7

scale estimation as part of Precise Orbit Determination: daily mean densities are averaged over 10 days.

The F30* model reproduces density significantly more accurately again, in particular for high levels of solar activity. The results of the comparisons with the three density datasets are listed in Table 2. The F30* model is more accurate at the three altitudes and for all investigated low and high activity periods. The two columns on the right present the mean and standard deviation of F10.7 and F30*, and the standard deviation of the detrended flux. Two main differences are revealed: the F30* 81-day mean flux is higher than F10.7 and especially so for 2010–2015 and the detrended flux is less variable (i.e. the amplitudes of the flux at the solar rotation period and less are smaller).

7. Conclusions

We have shown that the solar radio flux at 30 cm is a valuable alternative to the better known F10.7 index. Both offer the same radiometric stability and continuity, and have been measured for several decades on a daily basis. The 30 cm flux contains a relatively larger proportion of emissions coming from solar features such as plages, faculae and hot coronal loops, and consequently correlates better than F10.7 with the MgII core-to-wing index. Multiscale comparisons with the thermospheric density reveal the superior performance of 30 cm flux and the MgII index over the F10.7 index. We emphasise the importance of performing such comparisons scale-wise, because these proxies do not all correlate equally well at all time scales.

Thermosphere models constructed with the 30 cm and the 10.7 cm flux but otherwise identical density data demonstrate the better performance of the model based on the 30 cm flux – on average. This better performance is achieved for all three density datasets, at three altitudes, and covering solar cycle minimum to maximum conditions. Notice that none of the GOCE, GRACE and Stella data after 2010 were used in the model construction, i.e. they can be considered as independent data. Table 2 and Figures 7–9 reveal that the 30 cm flux makes a more accurate density modelling possible:

- on the whole, as the bias (0–20% smaller) and their standard deviations (15–40% smaller) of the density ratios imply;
- on time scales of years, e.g. the smaller bias after 2010 with GRACE and Stella, or before 2002 with Stella;
- at the solar rotation period of about 27 days, for which the smaller modulation amplitude (as compared to that obtained by using F10.7) leads to smaller residual errors. The differenced density ratio ($\Delta(O/C)$) is 35–50% smaller.

Unexpectedly, the full modelling exercise gives more convincing results with the 30 cm flux than what the spectral analysis suggests in Section 5. We suspect that this is due to the lower accuracy of the mean densities, and also because they do not cover all the years with the largest differences between the 30 cm flux and F10.7, specifically from 2012 to 2015.

Based on these results, we recommend using the 30 cm flux instead of the 10.7 cm flux for thermospheric modelling and to call it henceforth F30. Ultimately, more accurate descriptions of the solar forcing of the upper atmosphere should be based on direct UV measurements or on combinations of radio fluxes taken at different centimetric wavelengths (Tapping & Morton 2013). However, for the decade to come, the F30 index offers a powerful and radiometrically stable alternative that is of direct interest for space weather applications. A database with past values of F30, daily nowcasts and a 30-day prediction is available at https://spaceweather.cls.fr.

Acknowledgements. Part of this research was supported by CNES under Contract RTD-0167-CN. We thank the Penticton and Nobeyama radio observatories for making their excellent data available. The Nobeyama Radio Polarimeters are operated by Nobeyama Radio Observatory, a branch of National Astronomical Observatory of Japan. We also gratefully thank John Emmert (NRL) for providing us with the most recent neutral density mass data. This study made use of the CEDAR Database at the National Center for Atmospheric Research which is supported by the National Science Foundation. SOHO is a mission of international cooperation between ESA and NASA. The editor thanks two anonymous referees for their assistance in evaluating this paper.

References

Bendat, J.S., and A.G. Piersol. Random data analysis and measurement procedures. Wiley, London, New York, 2000.

BenMoussa, A., S. Gissot, U. Schühle, G. Del Zanna, and F. Auchère, et al. On-orbit degradation of solar instruments. *Sol. Phys.*, **288**, 389–434, 2013, DOI: 10.1007/s11207-013-0290-z.

Bowman, B.R., W.K. Tobiska, F. Marcos, and C. Valladares. The JB2006 empirical thermospheric density model. *J. Atmos. Sol. Terr. Phys.*, **70**, 774–793, 2008, DOI: 10.1016/j.jastp.2007.10.002.

Bowman, B.R., W.K. Tobiska, and F.A. Marcos. The development of new solar indices for use in thermospheric density modeling, In: *AIAA/AAS Astrodynamics Specialist Conference and Exhibit (Keystone, CO)*. **vol. AIAA 2006-6165**, AAS Publications Office, San Diego, 1–13, 2006.

Bruinsma, S. The DTM-2013 thermosphere model. *J. Space Weather Space Clim.*, **5 (27)**, A1, 2015, DOI: 10.1051/swsc/2015001.

Bruinsma, S., G. Thuillier, and F. Barlier. The DTM-2000 empirical thermosphere model with new data assimilation and constraints at lower boundary: accuracy and properties. *J. Atmos. Sol. Terr. Phys.*, **65**, 1053–1070, 2003. DOI: 10.1016/S1364-6826(03)00137-8.

Bruinsma, S.L., E. Doornbos, and B.R. Bowman. Validation of GOCE densities and evaluation of thermosphere models. *Adv. Space Res.*, **54**, 576–585, 2014, DOI: 10.1016/j.asr.2014.04.008.

Dudok de Wit, T., and S. Bruinsma. Determination of the most pertinent EUV proxy for use in thermosphere modeling. *Geophys. Res. Lett*, **38 (19)**, L19102, 2011, DOI: 10.1029/2011GL049028.

Dudok de Wit, T., S. Bruinsma, and K. Shibasaki. Synoptic radio observations as proxies for upper atmosphere modelling. *J. Space Weather Space Clim.*, **4 (26)**, A06, 2014, DOI: 10.1051/swsc/2014003.

Dudok de Wit, T., M. Kretzschmar, J. Lilensten, and T. Woods. Finding the best proxies for the solar UV irradiance. *Geophys. Res. Lett.*, **36**, 10107, 2009, DOI: 10.1029/2009GL037825.

Dudok de Wit, T., L. Lefèvre, and F. Clette. Uncertainties in the sunspot numbers: estimation and implications. *Sol. Phys.*, **291 (9)**, 2709–2731, 2016, DOI: 10.1007/s11207-016-0970-6.

Emmert, J.T. A long-term data set of globally averaged thermospheric total mass density. *J. Geophys. Res. [Space Phys]*, **114**, A06315, 2009, DOI: 10.1029/2009JA014102.

Emmert, J.T. Altitude and solar activity dependence of 1967–2005 thermospheric density trends derived from orbital drag. *J. Geophys. Res. [Space Phys]*, **120**, 2940–2950, 2015a, DOI: 10.1002/2015JA021047.

Emmert, J.T. Thermospheric mass density: a review, *Adv. Space Res.*, **56**, 773–824, 2015b, DOI: 10.1016/j.asr.2015.05.038.

Ermolli, I., K. Shibasaki, A. Tlatov, and L. van Driel-Gesztelyi. Solar cycle indices from the photosphere to the corona: measurements and underlying physics. *Space Sci. Rev.*, **186 (1–4)**, 105–135, 2014, DOI: 10.1007/s11214-014-0089-8.

Floyd, L., J. Newmark, J. Cook, L. Herring, and D. McMullin. Solar EUV and UV spectral irradiances and solar indices. *J. Atmos. Sol. Terr. Phys.*, **67**, 3–15, 2005, DOI: 10.1016/j.jastp.2004.07.013.

Gary, D.E., and C.U. Keller. *Solar and space weather radiophysics – current status and future developments*. Astrophysics and Space Science Library, **vol. 314**, Kluwer Academic Publishers, Dordrecht, 2004.

Hedin, A.E., C.A. Reber, G.P. Newton, N.W. Spencer, J.E. Salah, J.V. Evans, D.C. Kayser, D. Alcayde, P. Bauer, and L. Cogger. A global thermospheric model based on mass spectrometer and incoherent scatter data MSIS. I – N2 density and temperature. *J. Geophy. Res.*, **82**, 2139–2147, 1977, DOI: 10.1029/JA082i016p02139.

Hovestadt, D., M. Hilchenbach, A. Bürgi, B. Klecker, P. Laeverenz, et al. CELIAS – charge, element and isotope analysis system for SOHO. *Sol. Phys.*, **162**, 441–481, 1995, DOI: 10.1007/BF00733436.

Kundu, M.R. *Solar radio astronomy*, Interscience Publication, New York, 1965.

Lean, J.L., J.M. Picone, J.T. Emmert, and G. Moore. Thermospheric densities derived from spacecraft orbits: application to the Starshine satellites. *J. Geophys. Res. [Space Phys]*, **111 (A10)**, 4301, 2006, DOI: 10.1029/2005JA011399.

Lilensten, J., T. Dudok de Wit, M. Kretzschmar, P.-O. Amblard, S. Moussaoui, J. Aboudarham, and F. Auchère. Review on the solar spectral variability in the EUV for space weather purposes. *Ann. Geophys.*, **26**, 269–279, 2008, DOI: 10.5194/angeo-26-269-2008.

Pick, M., and N. Vilmer. Sixty-five years of solar radioastronomy: flares, coronal mass ejections and Sun Earth connection. *Astron. Astrophys. Rev.*, **16**, 1–153, 2008, DOI: 10.1007/s00159-008-0013-x.

Schmahl, E.J., M.R. Kundu. Synoptic radio observations. In: K.S. Balasubramaniam, J. Harvey, and D. Rabin, Editors. Synoptic solar physics, vol. 140 of Astronomical Society of the Pacific Conference Series, 387–399, 1998.

Tanaka, H. Toyokawa observatory. *Sol. Phys.*, **1**, 295–300, 1967, DOI: 10.1007/BF00150862.

Tapping, K.F. The 10.7 cm solar radio flux (F10.7). *Space Weather*, **11 (7)**, 394–406, 2013, DOI: 10.1002/swe.20064.

Tapping, K.F., and B. Detracey. The origin of the 10.7 CM flux. *Sol. Phys.*, **127**, 321–332, 1990, DOI: 10.1007/BF00152171.

Tapping, K.F., and D.C. Morton. The next generation of canadian solar flux monitoring. *J Phys.: Conf Ser*, **440 (1)**, 012039, 2013, DOI: 10.1088/1742-6596/440/1/012039.

Tobiska, W., S. Bouwer, and B. Bowman. The development of new solar indices for use in thermospheric density modeling. *J. Atmos. Sol. Terr. Phys.*, **70**, 803–819, 2008, DOI: 10.1016/j.jastp.2007.11.001.

Viereck, R., L. Puga, D. McMullin, D. Judge, M. Weber, and W.K. Tobiska. The Mg II index: a proxy for solar EUV. *Geophys. Res. Lett.*, **28**, 1343–1346, 2001, DOI: 10.1029/2000GL012551.

White, S.M., A.O. Benz, S. Christe, F. Fárnk, M.R. Kundu, et al. The relationship between solar radio and Hard X-ray Emission. *Space Sci. Rev.*, **159 (1–4)**, 225–261, 2011, DOI: 10.1007/s11214-010-9708-1.

White, S.M., and M.R. Kundu. Radio observations of gyroresonance emission from coronal magnetic fields. *Sol. Phys.*, **174**, 31–52, 1997, DOI: 10.1023/A:1004975528106.

Cite this article as: Dudok de Wit T & Bruinsma S. The 30 cm radio flux as a solar proxy for thermosphere density modelling. *J. Space Weather Space Clim.*, **7**, A9, 2017, DOI: 10.1051/swsc/2017008.